



## Catalytic combustion of chlorobenzene over MnO<sub>x</sub>–CeO<sub>2</sub> mixed oxide catalysts

Wang Xingyi <sup>\*</sup>, Kang Qian, Li Dao

Laboratory for Advanced Materials, Research Institute of Industrial Catalysis, East China University of Science and Technology, Shanghai 200237, PR China

### ARTICLE INFO

#### Article history:

Received 14 May 2008

Received in revised form 23 June 2008

Accepted 5 August 2008

Available online 22 August 2008

#### Keywords:

Chlorobenzene

MnO<sub>x</sub>–CeO<sub>2</sub>

CeO<sub>2</sub>

Catalytic combustion

### ABSTRACT

A series of MnO<sub>x</sub>–CeO<sub>2</sub> mixed oxide catalysts with different compositions prepared by sol–gel method were tested for the catalytic combustion of chlorobenzene (CB), as a model of volatile organic compounds of chlorinated aromatics. MnO<sub>x</sub>–CeO<sub>2</sub> catalysts with different ratios of Mn/Ce + Mn were found to possess high catalytic activity in the catalytic combustion of CB, and MnO<sub>x</sub>(0.86)–CeO<sub>2</sub> was identified as the most active catalyst, on which the temperature of complete combustion of CB was 254 °C. Effects of systematic variation of reaction conditions, including space velocity and inlet CB concentration on the catalytic combustion of CB were investigated. Additionally, the stability and deactivation of MnO<sub>x</sub>–CeO<sub>2</sub> catalysts were studied by various characterization methods and other assistant experiments. MnO<sub>x</sub>–CeO<sub>2</sub> catalysts with high Mn/Ce + Mn ratios present a stable high activity, which is related to their high ability to remove the adsorbed Cl species and a large amount of active surface oxygen.

© 2008 Elsevier B.V. All rights reserved.

### 1. Introduction

Chlorinated volatile organic compounds (CVOCs) in waste gases are released to the atmosphere from a wide range of industrial processes or the incineration of municipal and medical wastes. Direct thermal combustion, a conventional technology for the destruction of chlorinated organic compounds, usually requires temperatures exceeding 850–1000 °C and leads to the formation of small amounts of toxic polychlorinated aromatic compounds (i.e., polychlorinated dibenzodioxins [PCDDs] and dibenzofurans [PCDFs]), in addition to the standard products (i.e., CO, NO<sub>x</sub>, SO<sub>x</sub>) from combustion. Therefore, stringent environmental regulations are in place in several countries limiting PCDD/PCDF emissions [1].

So far as we are concerned, the catalytic oxidation of CVOCs to carbon dioxide, HCl, and water is the best method for their destruction. The major advantage of the catalytic combustion is that oxidation can be efficiently performed at temperatures between 250 and 550 °C and very dilute pollutants which cannot be thermally combusted without additional fuel can be treated efficiently. Therefore, a low-temperature catalytic combustion process offers significant cost saving when compared with the conventional thermal process.

Of studies of the catalysts for CVOC catalytic combustion, most have reported focusing on the three types of catalysts based on noble metals [2,3], transition metals [4,5] or zeolites [6,7]. Metal catalysts have been widely used because of their ability to catalyze oxidation, but they are susceptible to the deactivation by HCl and Cl<sub>2</sub>. The activities of zeolite are related to their acid properties. However, the problem of the formation of the by-product polychlorinated compounds on these catalysts is yet to be solved. Therefore, development of catalysts having high performance in converting CVOCs is of great interest.

In our previous work [8,9], CeO<sub>2</sub> as a catalyst for CVOCs catalytic combustion was discussed, and its activity was found higher than that of other reported catalysts [10–14], but deactivated quickly due to the strong adsorption of HCl or Cl<sub>2</sub> produced from the decomposition of CVOCs on CeO<sub>2</sub> surface to blockade the active sites. However, it is found if chlorine or chloride ions adsorbed on the CeO<sub>2</sub> surface was removed or transferred rapidly enough, the stability of CeO<sub>2</sub> catalyst could be improved and increased.

Among the catalysts for CVOCs catalytic combustion, including noble metals, transition metal oxides or solid acid catalysts, the transition metal oxide catalysts can resist the deactivation caused by chlorine poisoning. Manganese oxides, supported or unsupported, are used as important catalysts directly in the catalytic reactions [15–19], such as the oxidation of carbon monoxide, methane and hydrocarbons, the decomposition of ozone, N<sub>2</sub>O and H<sub>2</sub>O<sub>2</sub>, and the selective catalytic reduction (SCR) of NO. The presence of Mn in Mn–Ce–O or Mn–Cu–O mixed oxide catalysts can enhance their catalytic activities for CO oxidation and SCR of NO.

\* Corresponding author at: P.O. 396, East China University of Science and Technology, 130 Meilonglu, Shanghai 200237, PR China. Tel.: +86 21 64253372; fax: +86 21 64253372.

E-mail address: [wangxy@ecust.edu.cn](mailto:wangxy@ecust.edu.cn) (W. Xingyi).

In the present work, the mixed oxide catalysts,  $\text{MnO}_x\text{-CeO}_2$ , prepared by sol-gel method, were tested in catalytic combustion of CB, and the effects of Mn amount in catalysts, operation conditions of space velocity and inlet CB concentration on catalytic activity were investigated. Additionally, the possible cause of catalyst deactivation was discussed based on the data from stability of  $\text{MnO}_x\text{-CeO}_2$  catalysts and thus investigated by assistant experiments.

## 2. Experimental

### 2.1. Catalysts preparation

$\text{MnO}_x\text{-CeO}_2$  mixed oxides,  $\text{MnO}_x$  and  $\text{CeO}_2$  were prepared by sol-gel method: an aqueous solution containing  $\text{Mn}(\text{NO}_3)_2$ ,  $\text{Ce}(\text{NO}_3)_3\cdot 6\text{H}_2\text{O}$  (SCRC, 99.0%), and citric acid (citric acid/  $(\text{Mn} + \text{Ce}) = 0.3$ , molar ratio) was gradually heated to 50 °C and kept at this temperature for 1.5 h with stirring, resulting in the formation of yellowish gel. It was then dried at 110 °C for 12 h and calcined at 550 °C for 5 h in air.  $\text{Mn}/\text{Ce} + \text{Mn}$  ratio in  $\text{MnO}_x\text{-CeO}_2$  is denoted as  $\text{MnO}_x(X)\text{-CeO}_2$  in the text.

### 2.2. Catalysts characterization

#### 2.2.1. Powder X-ray diffraction pattern

The powder X-ray diffraction patterns (XRD) of the samples were recorded on a Rigaku D/Max-rC powder diffractometer using  $\text{Cu K}\alpha$  radiation (40 kV and 100 mA). The diffractograms were recorded within the  $2\theta$  range of 10–80° with a  $2\theta$  step size of 0.01° and a step time of 10 s.

#### 2.2.2. Nitrogen adsorption/desorption

The nitrogen adsorption and desorption isotherms were measured at –196 °C on an ASAP 2400 system in static measurement mode. The samples were outgassed at 160 °C for 4 h before the measurement. The specific surface area was calculated using the BET model.

#### 2.2.3. Thermogravimetric analysis

Coke formation on the catalyst was evaluated with thermogravimetric analysis (TGA) using a PerkinElmer Pyris Diamond TG/TGA Setaram instrument. The fresh and used  $\text{MnO}_x\text{-CeO}_2$  samples were heated up to 800 °C from room temperature (heating rate of 10 °C min<sup>–1</sup>) in a  $\text{N}_2/\text{O}_2$  stream.

#### 2.2.4. X-ray photoelectron spectroscopy

The XPS measurements were made on a VG ESCALAB MK II spectrometer by using  $\text{Mg K}\alpha$  (1253.6 eV) radiation as the excitation source. Charging of samples was corrected by setting the binding energy of adventitious carbon (C 1s) at 284.6 eV. The powder sample, pressed into self-supporting disks, was loaded into a sub-chamber and then evacuated for 4 h, prior to the measurements at 25 °C.

#### 2.2.5. Temperature programming reduction

$\text{H}_2$ -temperature programming reduction ( $\text{H}_2\text{-TPR}$ ) was investigated by heating  $\text{MnO}_x\text{-CeO}_2$  samples (150 mg) in  $\text{H}_2$  (5 vol.%) /Ar flow (30 ml min<sup>–1</sup>) at a heating rate of 10 °C min<sup>–1</sup> from 20 to 750 °C. The hydrogen consumption was monitored by thermocconductivity detector (TCD). Before the  $\text{H}_2\text{-TPR}$  analysis, the samples were heated for 60 min in Ar flow at 500 °C, and then treated in  $\text{O}_2$  at room temperature for 30 min.

#### 2.2.6. Raman spectroscopy

The Raman spectra were obtained on a Renishaw in Viat + Reflex spectrometer equipped with a CCD detector at ambient

temperature and moisture-free conditions. The emission line at 514.5 nm from an  $\text{Ar}^+$  ion laser (Spectra Physics) was focused, analyzing spot about 1 mm, on the sample under the microscope. The power of the incident beam on the sample was 3 mW. Time of acquisition was varied according to the intensity of the Raman scattering. The wave numbers obtained from spectra were accurate to within 2 cm<sup>–1</sup>.

### 2.3. Catalytic activity measurement

Catalytic combustion reactions were carried out at atmospheric pressure in a continuous flow micro-reactor made of a quartz tube of 4 mm in inner diameter. 200 mg catalyst was packed at the bed of the reactor. The feed flow through the reactor was set with the concentration of CB 1000 ppm and the gas hourly space velocity (GHSV) at 15,000 h<sup>–1</sup>. The feed stream to reactor was therefore prepared by delivering liquid CB with a syringe pump into dry air, which was metered by a mass flow controller. The injection point was electrically heated to ensure the complete evaporation of CB. The temperature of reaction was measured and controlled with a thermocouple located just at the hot spot of the reactor bed. The effluent gases were analyzed on-line at a given temperature by using two gas chromatographs (GC), one equipped with FID for the quantitative analysis of the organic chlorinated reactant, and the other with TCD for the quantitative analysis of CO and  $\text{CO}_2$ . The concentrations of  $\text{Cl}_2$  and HCl were analyzed by the effluent stream bubbling through a 0.0125N NaOH solution, and chlorine concentration was then determined by the titration with ferrous ammonium sulphate (FAS) using *N,N*-diethyl-*p*-phenylenediamine (DPD) as indicator [20]. The concentration of chloride ions in the bubbled solution was determined by using a chloride ion selective electrode [21].

## 3. Results and discussion

### 3.1. Catalyst characterization

Wide angle XRD patterns of  $\text{MnO}_x\text{-CeO}_2$  catalysts with different ratios of  $\text{Mn}/(\text{Mn} + \text{Ce})$  are shown in Fig. 1. The diffractogram of  $\text{CeO}_2$  shows the diffraction peaks (at 28.6°, 33.3°, 47.5°, 56.5° and 59.2°) of cerianite characterized with a fluorite-like structure. A more asymmetric shape of such reflections with a lower intensity confirms the weakening degree of the crystallinity of samples with  $\text{Mn}/(\text{Mn} + \text{Ce})$  ratio from 0.13 to 0.86, which is consistent with the increase in surface area (see Table 1). Indeed, the fact that the average particle size of ceria, calculated from the peak at 28.6° of (1 1 1) crystal plane, is inversely related to the surface area (see Table 1), which denotes main contribution of the matrix to surface area exposure.

Moreover, the diffraction peaks of cubic fluorite-like structure of  $\text{MnO}_x\text{-CeO}_2$  catalysts shift to slightly higher values of Bragg angles in the range of 28.7–29.0°, indicating that part of manganese species can enter into the fluorite lattice to form  $\text{MnCeO}_x$  solid solutions [22]. As reported in Ref. [23], the ionic radius of  $\text{Mn}^{3+}$  (0.066 nm) is smaller than that of  $\text{Ce}^{4+}$  (0.094 nm), and the incorporation of  $\text{Mn}^{3+}$  into the fluorite lattice results in the decrease in the lattice parameters, which is justified by the results shown in Table 1. It can be seen that appreciable decrease of ceria particle size parallels with an increase in the Mn amount. In addition to the reflections of the cerianite, the diffractograms of  $\text{MnO}_x\text{-CeO}_2$  catalysts with  $\text{Mn}/(\text{Mn} + \text{Ce})$  ratio higher than 0.78 show two small peaks at 32.9° and 37.2°, indexes of incipient  $\alpha\text{-Mn}_2\text{O}_3$  crystallization in the form of bixbyite [24] and  $\text{MnO}_2$  crystallization in the form of pyrolusite [25,26], respectively. For  $\text{MnO}_x(0.94)\text{-CeO}_2$  sample, the reflections of  $\text{CeO}_2$  almost dis-

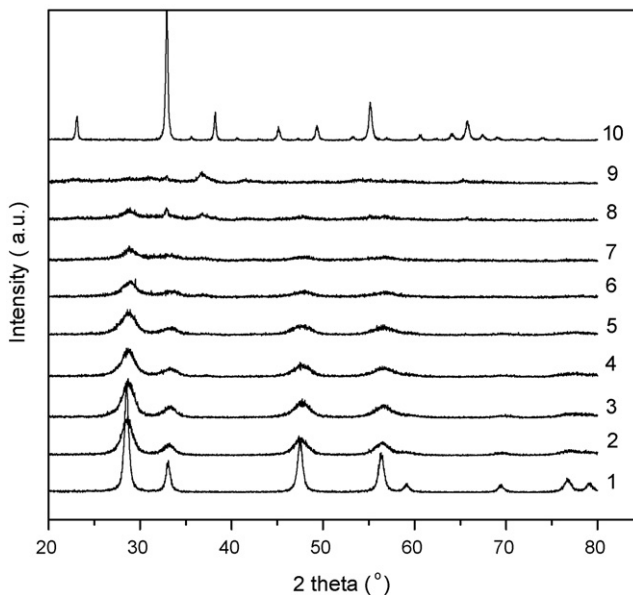


**Fig. 1.** XRD patterns of the  $\text{MnO}_x\text{-CeO}_2$  catalysts with different ratios of  $\text{Mn}/(\text{Ce} + \text{Mn})$ : (1)  $\text{CeO}_2$ ; (2) 0.13; (3) 0.27; (4) 0.39; (5) 0.50; (6) 0.69; (7) 0.78; (8) 0.86; (9) 0.93; (10)  $\text{MnO}_x$ .

appear, due to a high dispersion of Ce species into  $\text{MnO}_x$  matrix. For pure  $\text{MnO}_x$  sample, there appear only strong reflections from  $\alpha\text{-Mn}_2\text{O}_3$  phase.

XPS results (shown in Table 2) confirm the coexistence of three kinds of Mn species,  $\text{Mn}^{2+}$ ,  $\text{Mn}^{3+}$  and  $\text{Mn}^{4+}$  [27], on the surface of all containing-Mn catalysts. The fact that the samples with  $\text{Mn}/(\text{Mn} + \text{Ce})$  ratio less than 0.78 cannot present the reflects of  $\text{MnO}_2$ ,  $\alpha\text{-Mn}_2\text{O}_3$  and  $\text{MnO}$  phases may be due either to the formation of  $\text{MnCeO}_x$  'solid solutions' with cubic fluorite structure or to the occurrence of very small crystals of manganese oxides.

The results of TPR analyses for  $\text{MnO}_x\text{-CeO}_2$  catalysts are shown in Fig. 2. Two peaks on TPR profiles result from the reduction of Mn ions belonging to different structures/phases.  $\text{H}_2\text{-TPR}$  profile of pure  $\text{MnO}_x$  shows two overlapped strong reduction peaks with maximums at 380 and 480 °C, respectively. Assuming that  $\text{MnO}$  is the final reduction state [28] from various Mn species in the initial  $\text{MnO}_x$ , it is reasonable to propose that the peak at low temperature could be assigned to the reduction of  $\text{MnO}_2/\text{Mn}_2\text{O}_3$  to  $\text{Mn}_3\text{O}_4$ , and the peak at high temperature corresponds to the combined reduction of  $\text{Mn}_3\text{O}_4$  to  $\text{MnO}$  [29–31] and surface oxygen removal of ceria.

The reduction of pure  $\text{CeO}_2$  occurs at 517 °C in the range of experimental temperature, associated with the reduction of surface  $\text{Ce}^{4+}$  ions [26], consuming less  $\text{H}_2$  as compared with the

reduction features of pure  $\text{MnO}_x$ . With the addition of Mn into  $\text{CeO}_2$ , the reduction temperatures of  $\text{MnO}_x\text{-CeO}_2$  catalysts systematically shift to lower values.  $\text{H}_2\text{-TPR}$  profiles of  $\text{MnO}_x(0.27)\text{-CeO}_2$  and  $\text{MnO}_x(0.50)\text{-CeO}_2$  with a lower amount of Mn exhibit two broad reduction peaks around 260 and 350 °C, respectively. The former can be related to the presence of "isolated"  $\text{Mn}^{4+}$  ions which "embedded" into the surface defective positions of the ceria lattice. The latter can be assigned to the reduction of  $\text{Mn}^{3+}$  species. Their reduction is promoted by a high degree of coordinative unsaturation and, perhaps, by neighboring  $\text{Ce}^{4+}$  ions, which, in turn, undergo reduction to  $\text{Ce}^{3+}$  species [32]. On  $\text{MnO}_x(0.69)\text{-CeO}_2$ ,  $\text{MnO}_x(0.86)\text{-CeO}_2$ , and  $\text{MnO}_x(0.92)\text{-CeO}_2$  catalysts, the reduction peak at 260 °C still occur as a shoulder, indicating the presence of "isolated"  $\text{Mn}^{4+}$  ions. Moreover, the peak centered at about 322 °C appears, which is related to the first step reduction of very small  $\text{MnO}_2$  particles well-dispersed across the ceria matrix [26], and the second step reduction occurs at higher temperature, due to the gradual decrease of the amount of Ce species. These results indicate that two kinds of  $\text{Mn}^{4+}$  species present in  $\text{MnO}_x\text{-CeO}_2$  catalyst, i.e., "isolated"  $\text{Mn}^{4+}$  and  $\text{Mn}^{4+}\text{-O-Ce}^{4+}$  for catalysts with both high and low ratios of  $\text{Mn}/(\text{Ce} + \text{Mn})$ , and highly dispersed  $\text{MnO}_2$  particles in  $\text{CeO}_2$  mainly for the catalysts with high Mn amount.

Fig. 3 presents XPS measurement of O 1s core level of oxygen species on the catalyst surface, and the data are summarized in Table 2. O 1s spectrum of  $\text{CeO}_2$  has two peaks at 528.9–530 eV, assigned to lattice oxygen. Two shoulder peaks at ca. 531.9 and 533.5 eV are observed, which can be attributed to adsorbed oxygen and weakly bonded oxygen species (active oxygen) [33], and to surface oxygen by hydroxyl species and adsorbed water species presser as contaminants at the surface, respectively. O 1s core level of lattice oxygen on  $\text{MnO}_x\text{-CeO}_2$  catalysts shifts to high values because of " $\text{Mn} \leftarrow \text{O}$ " electron-transfer processes [26]. Meanwhile, the amount of lattice oxygen decreases. With the increase in the  $\text{Mn}/(\text{Mn} + \text{Ce})$  ratio from 0.27 to 0.50, the level of active oxygen on the surface of catalysts decreases from 531.9 to 531.3 eV, which is similar to that of  $\text{MnO}_x$ . However, the amount of active oxygen increases with the increase in the  $\text{Mn}/(\text{Ce} + \text{Mn})$  ratio (see Table 1), hence leading to the increase in  $\text{H}_2$  consumptions in  $\text{H}_2\text{-TPR}$ , as indicated in Fig. 2 (according to the area under  $\text{H}_2\text{-TPR}$  profile). This phenomena is in line with the results obtained by Arena [26], who found that " $\text{Mn} \leftarrow \text{O}$ " electron-transfer processes enable the formation of very reactive electrophilic oxygen species (e.g.,  $\text{O}_2^-$ ,  $\text{O}_2^{=}$ ,  $\text{O}^-$ ,  $\text{O}^*$ ) that are active oxygen species.

### 3.2. Activity tests

In order to check whether or not some reactions under thermal combustion condition could take place, "blank test" was carried out, with 3 mm crushed quartz glass (40–60 mesh) packed in the

**Table 1**  
The properties of the catalysts under study

Mn content (at.%)	$d_{111}(\text{CeO}_2)$ (Å)	Surface area ( $\text{m}^2/\text{g}$ )	Ceria particle size $d_{\text{CeO}_2}$ (nm) <sup>a</sup>	Lattice parameter (Å)
CeO <sub>2</sub>	3.1250	9	13.9	5.41
13	3.1293	48	6.7	5.42
27	3.1190	51	6.2	5.39
39	3.1110	52	6.1	5.39
50	3.1100	53	5.9	5.39
69	3.0785	63	5.8	5.33
78	3.0974	62	5.6	5.36
86	3.0889	65	5.6	5.35
94	3.0932	64	–	5.35
MnO <sub>x</sub>	–	9	–	–

<sup>a</sup> From the Scherrer equation, applied to the  $\langle 111 \rangle$  reflection of the cerianite.

**Table 2**

Summary of the results of XPS analysis

Catalysts	Mn/Mn + Ce <sup>a</sup> (%)	Mn/Mn + Ce <sup>b</sup> (%)	Mn (%)	Ce (%)	O (%)	Mn distribution (%)			Oxygen distribution (%)		
						Mn <sup>4+</sup>	Mn <sup>3+</sup>	Mn <sup>2+</sup>	O <sub>latt</sub>	O <sub>sur</sub>	O <sub>ads</sub>
CeO <sub>2</sub>	0	0	0	35.8	64.2	–	–	–	51.5	10.4	2.3
MnOx(0.27)–CeO <sub>2</sub>	27	20.0	6.8	26.2	67.1	2.3	2.8	0.8	52.4	11.7	2.9
MnOx(0.50)–CeO <sub>2</sub>	50	55.0	19.4	15.8	64.8	6.2	9.1	3.5	44.3	14.5	3.9
MnOx(0.69)–CeO <sub>2</sub>	69	68.6	24.5	11.2	64.3	7.1	10.9	4.1	40.0	20.3	3.0
MnOx(0.78)–CeO <sub>2</sub>	78	73.4	26.9	9.6	63.5	7.1	12.5	4.7	39.8	21.2	2.5
MnOx(0.86)–CeO <sub>2</sub>	86	79.8	30.2	7.7	62.1	9.8	12.8	4.4	41.1	20.1	0.9
MnOx	100	100	32.1	–	67.9	11.1	12.3	7.3	44.9	19.8	3.2

<sup>a</sup> The composition of Mn in the preparation.<sup>b</sup> The value estimated by XPS analysis.

reactor. As shown in Fig. 4, low conversion of CB without catalyst can only occurs above 450 °C. Can Li [34] found no significant oxidation of CB at temperature up to 500 °C in a blank reactor experiment.

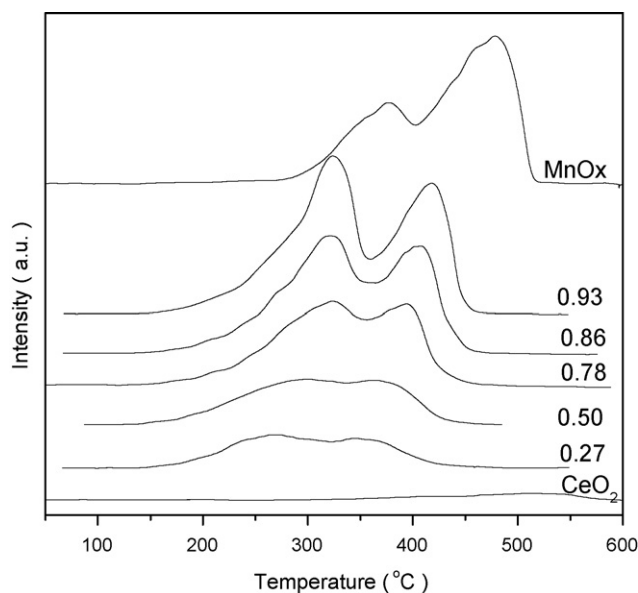
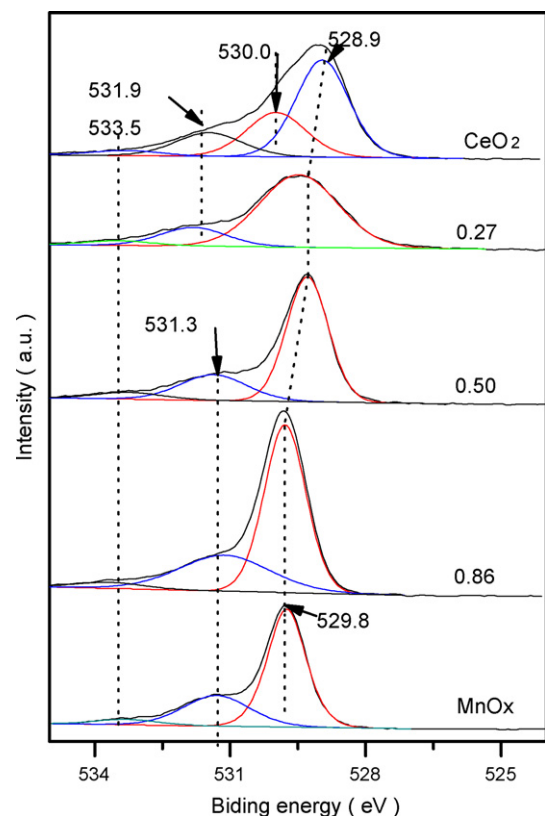
MnOx–CeO<sub>2</sub> catalysts appear to be superior for CB catalytic combustion, of which MnOx–CeO<sub>2</sub> catalysts with Mn/Mn + Ce ratio in the range from 0.78 to 0.94 have the best activity, and the complete combustion of CB over the catalysts proceeds at GHSV 15,000 h<sup>-1</sup> at about 254 °C, the temperature being much lower than all those catalysts reported in previous literatures, including noble metal-based catalysts [35–37] or MnOx/TiO<sub>2</sub>–Al<sub>2</sub>O<sub>3</sub> and TiO<sub>2</sub> catalysts [34,38]. With the decrease of Mn/Mn + Ce ratio, the activity of MnOx–CeO<sub>2</sub> catalysts reduces. Fig. 5 shows  $T_{50\%}$  and  $T_{99\%}$  (the temperature needed for the conversion of 50 and 99%, respectively) as the functions of Mn amount; the activity of catalysts increases as the Mn amount increases, except the case of MnOx.

Over pure MnOx, the conversion of CB reaches 99% at 471 °C, higher than that over the MnOx–CeO<sub>2</sub> catalysts, exclusive of the case of MnOx(0.27)–CeO<sub>2</sub>. CeO<sub>2</sub> presents a higher activity at the initial stage than MnOx. However, it deactivates gradually as the conversion of CB drops from 25% at 200 °C to 8% at 300 °C. With the further increase of temperature, the conversion of CB on CeO<sub>2</sub> increases gradually, and reaches 99% at 600 °C, much higher than the temperature for total conversion of trichloroethylene on CeO<sub>2</sub> [9]. The incorporation of MnOx into CeO<sub>2</sub> improves the activity and stability of catalysts, depending on Mn/Ce + Mn ratio. For

MnOx(0.13)–CeO<sub>2</sub>,  $T_{50\%}$  reduces to 240 °C from 438 °C for CeO<sub>2</sub> and its deactivation occurs at higher temperature. With the increase in Mn amount, MnOx–CeO<sub>2</sub> catalysts become more stable in activity.

### 3.3. Effect of space velocity on CB catalytic combustion

The catalytic processes for VOCs treatment usually require a gas space velocity (GHSV) as high as 10,000–30,000 h<sup>-1</sup>. Fig. 6 shows the conversion of CB over MnOx–CeO<sub>2</sub> catalysts as the function of reaction temperature at GHSV of 30,000 h<sup>-1</sup>. MnOx–CeO<sub>2</sub> catalysts with Mn/Mn + Ce ratio of 0.50, 0.78 and 0.86 present a lower conversion of CB, as compared with the condition at GHSV of 15,000 h<sup>-1</sup> shown in Fig. 4, because the residence time for reactants through the bed decreases and thus high temperature is needed to achieve a sufficient conversion at a higher space velocity. The temperature for 90% conversion of CB must be kept at 280 °C at GHSV of 30,000 h<sup>-1</sup>, 45 °C higher than that at GHSV of 15,000 h<sup>-1</sup>. However, the cases of pure oxides, MnOx and CeO<sub>2</sub>, are different.

Fig. 2. TPR profiles of the MnOx–CeO<sub>2</sub> catalysts with different ratios of Mn/Mn + Ce.Fig. 3. O 1s XPS spectra for the MnOx–CeO<sub>2</sub> catalysts with different ratios of Mn/Mn + Ce.

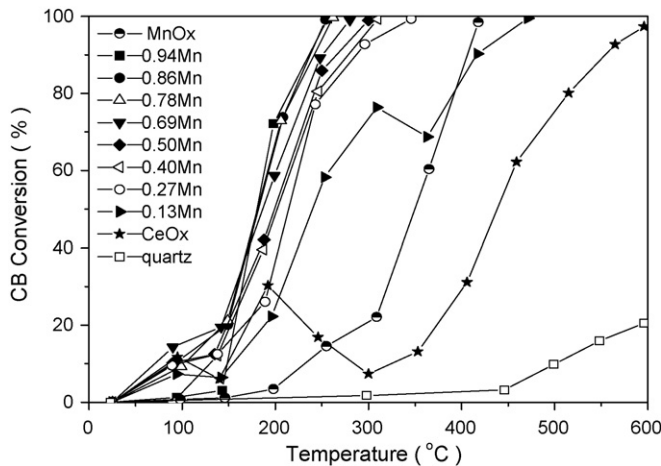


**Fig. 4.** The activity of the fresh MnOx–CeO<sub>2</sub> catalysts with different ratios of Mn/Mn + Ce for CB catalytic combustion, gas composition: 1000 ppm CB, 10% O<sub>2</sub>, N<sub>2</sub> balance; GHSV = 15,000 h<sup>-1</sup>.

The effect of GHSV on the conversion of CB over MnOx is little significant in the range of 100–360 °C, probably resulting from a low reaction rate, while 90% conversion at GHSV of 30,000 h<sup>-1</sup> is reached at 444 °C, 38 °C higher than that at GHSV of 15,000 h<sup>-1</sup>. The conversion over CeO<sub>2</sub> catalyst becomes lower at GHSV of 30,000 h<sup>-1</sup> at low temperature, but the section of conversion curve at more than 300 °C shifts systematically to lower temperature by about 50 °C. The removal of Cl species adsorbed on CeO<sub>2</sub> surface which results in the deactivation of CeO<sub>2</sub> (relative discussion shown in later text) may be facilitated by high flow of feed stream. So, the fact that the conversion over CeO<sub>2</sub> catalyst increases at GHSV of 30,000 h<sup>-1</sup> may be related to the reduction of Cl species adsorbed.

#### 3.4. Effect of inlet CB concentration on CB catalytic combustion

The effect of inlet CB concentration on the conversion of CB over MnOx(0.86)–CeO<sub>2</sub> catalyst at the space velocity of 15,000 h<sup>-1</sup> was investigated. Fig. 7 shows the conversion curves for catalytic combustion of CB with different inlet concentrations. It can be seen that the conversion of CB has a mild variation with the increase in the inlet CB concentration from 500 to 1500 ppm, and even at low

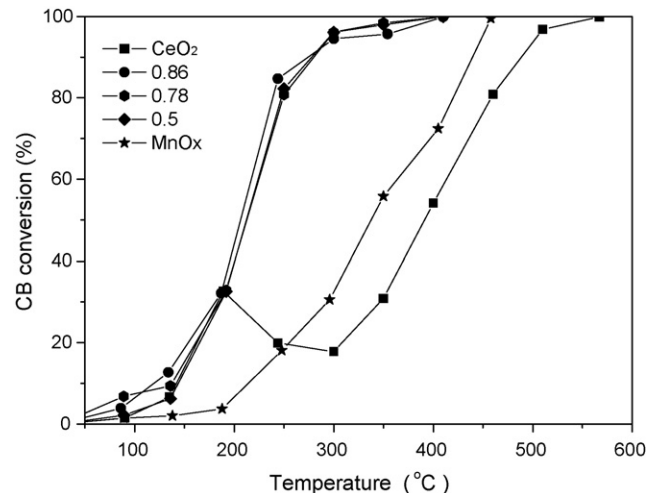


**Fig. 6.** The activity of the fresh MnOx–CeO<sub>2</sub> catalysts with different ratios of Mn/Mn + Ce for CB catalytic combustion, gas composition: 1000 ppm CB, 10% O<sub>2</sub>, N<sub>2</sub> balance; GHSV = 30,000 h<sup>-1</sup>.

concentration of CB, MnOx(0.86)–CeO<sub>2</sub> catalyst still shows higher activity. Therefore, MnOx(0.86)–CeO<sub>2</sub> catalyst may be used for treating the emission containing CB. Within  $\pm 1.5\%$  of the average deviation of CB concentration, the dependence of reaction rate on CB concentration over MnOx(0.86)–CeO<sub>2</sub> catalyst is less significant. Experimental determination shows that the complete oxidation of CB is first-order in CB concentration. The fact that CB conversion increases slightly with the decrease of CB inlet concentration from 1500 to 500 ppm is related to a slight deactivation of MnOx(0.86)–CeO<sub>2</sub> catalyst in higher CB concentration. Corella and Padilla [39] also reported the same results in trichloroethylene combustion.

#### 3.5. The analyses of products

Within the application limits of FID, all the catalysts studied in this experiment provide more than 99.5% selectivity to carbon oxides (more than 98% CO<sub>2</sub> and trace CO) and no polychlorinated benzene or other detectable C-containing by-products are found. This is very different from the case for noble metal-based catalysts [34–36], over which a substantial amount of polychlorinated benzene is formed during the catalytic combustion of CB. Cl balance gives 15–20% less amount in the outlet stream than in the

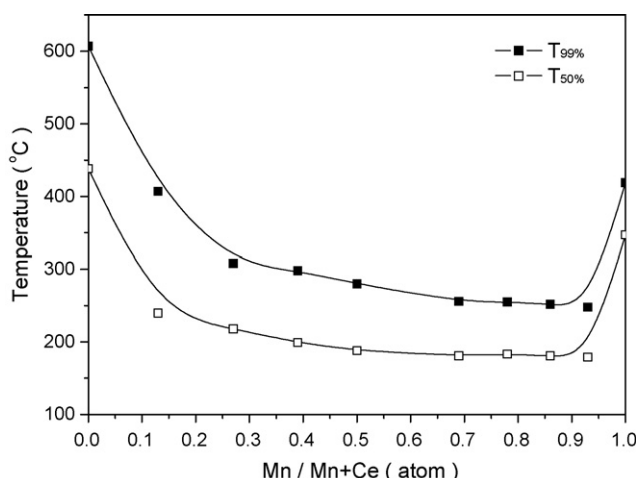


**Fig. 5.** The T<sub>50%</sub> and T<sub>99%</sub> for CB catalytic combustion over the MnOx–CeO<sub>2</sub> catalysts, gas composition: 1000 ppm CB, 10% O<sub>2</sub>, N<sub>2</sub> balance; GHSV = 15,000 h<sup>-1</sup>.

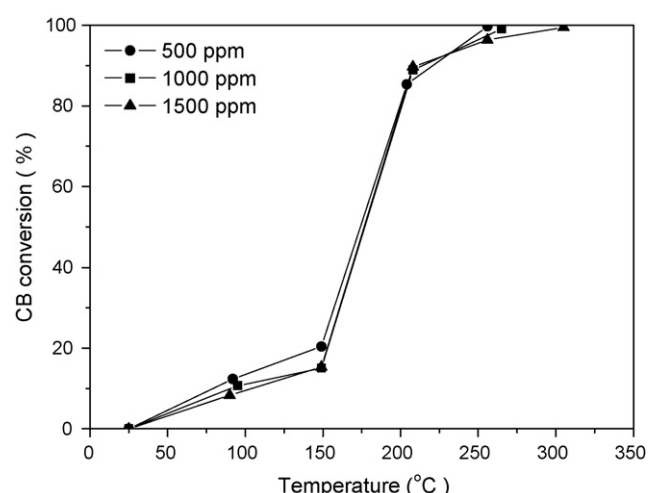


**Fig. 7.** The effect of CB concentration on the activity of MnOx(0.86)–CeO<sub>2</sub>(B) catalyst, gas composition: 1000 ppm CB, 10% O<sub>2</sub>, N<sub>2</sub> balance; GHSV = 15,000 h<sup>-1</sup>.

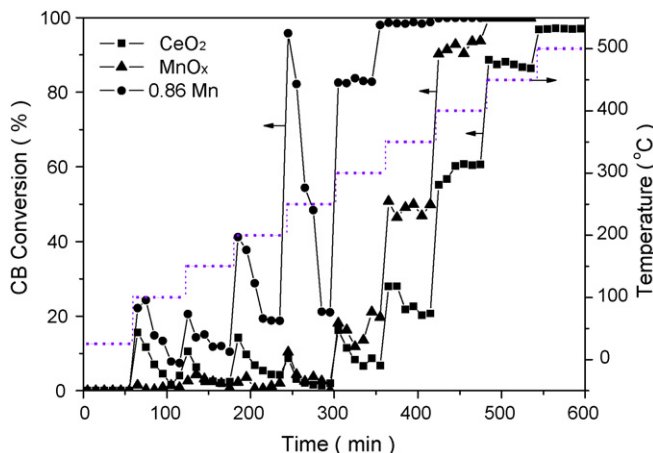


Fig. 8. The stability of catalysts for CB catalytic combustion at different temperature, gas composition: 1000 ppm CB, 10% O<sub>2</sub>, N<sub>2</sub> balance; GHSV = 15,000 h<sup>-1</sup>.

inlet stream; this fact means that deposition of Cl species occurs on the surface of catalysts.

### 3.6. Catalyst deactivation

For the catalytic combustion of CVOCs, the catalyst deactivation is still a hurdle in commercial applications. In previous work, CeO<sub>2</sub> was found rapidly deactivated due to strong adsorption of Cl on active sites during the catalytic combustion of trichloroethylene [9]. In this work, the stability of MnOx(0.86)–CeO<sub>2</sub>, MnOx and CeO<sub>2</sub> was investigated for the catalytic combustion of CB. Results from the tests conducted at the stepwise-varied temperatures from 50 to 500 °C are presented in Fig. 8, and the variation in activities was observed in 60 min at a given temperature. Conversion of CB vs. reaction temperature and reaction time was plotted.

As shown, CeO<sub>2</sub> presents an unstable activity and the activity drops quickly as the reaction temperature rises in the range of 100–200 °C, but this drop becomes less obvious in the range of 250–350 °C, probably due to fairly low activity. At higher than 350 °C, CeO<sub>2</sub> achieves a low stable activity without a substantial decrease in conversion.

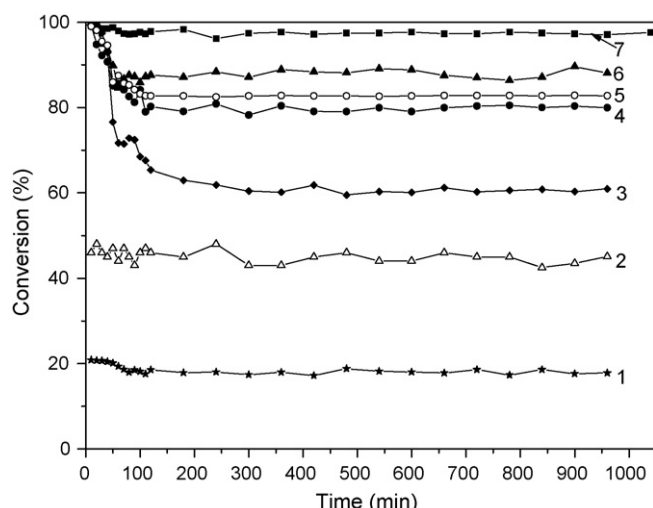


Fig. 9. The stability tests of catalysts with different ratios of Mn/Mn + Ce at 350 °C; (1) CeO<sub>2</sub>; (2) MnOx; (3) 0.27; (4) 0.5; (5) 0.69; (6) 0.78; (7) 0.86; gas composition: 1000 ppm CB, 10% O<sub>2</sub>, N<sub>2</sub> balance; GHSV = 15,000 h<sup>-1</sup>.

On the contrary, there is not a significant drop in the activity observed on MnOx, although MnOx shows fairly low activity. The activity of MnOx(0.86)–CeO<sub>2</sub> is improved really at various temperatures, but its activity is not stable until 300 °C. The range of temperature within which MnOx(0.86)–CeO<sub>2</sub> and CeO<sub>2</sub> catalysts drop activity significantly is almost the same one, i.e., 125–300 °C.

Additionally, compared with the results shown in Fig. 4, it can be seen that the conversion of CB over CeO<sub>2</sub> and MnOx(0.86)–CeO<sub>2</sub> at different temperature steps decreases to some extent (see Fig. 8). The data in Fig. 4 were obtained by analyses of effluent gases at a given temperature (to maintain 10 min) on-line by using gas chromatographs. The time of each test run for a catalyst to maintain in the feed stream is so short that the amount of Cl adsorbed on the catalyst surface is small. Therefore, the activity of catalysts is similar to one of fresh catalysts at different temperature. During the test for obtaining the results shown in Fig. 8, the activity of every catalyst was evaluated for 60 min at every temperature step in the range of 50–500 °C. The deactivation at different temperature steps is more serious. It seems reasonable that Fig. 8 shows a lower CB conversion over CeO<sub>2</sub> and MnOx(0.86)–CeO<sub>2</sub> than Fig. 4.

For practical use, the stability in catalytic activity is essential. Fig. 9 presents the experimental results of the stability test at

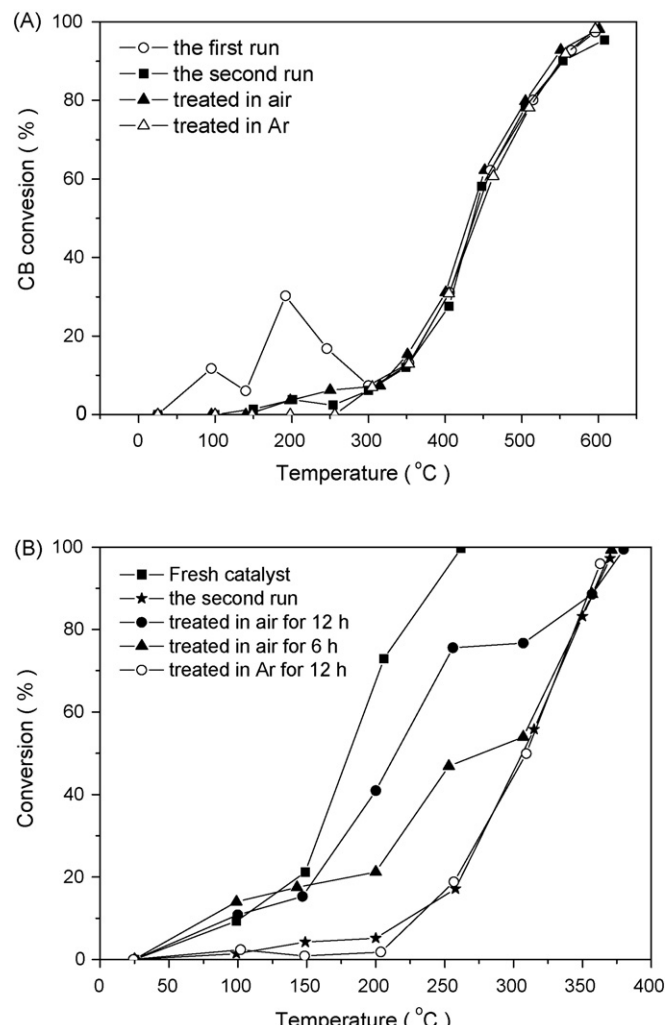
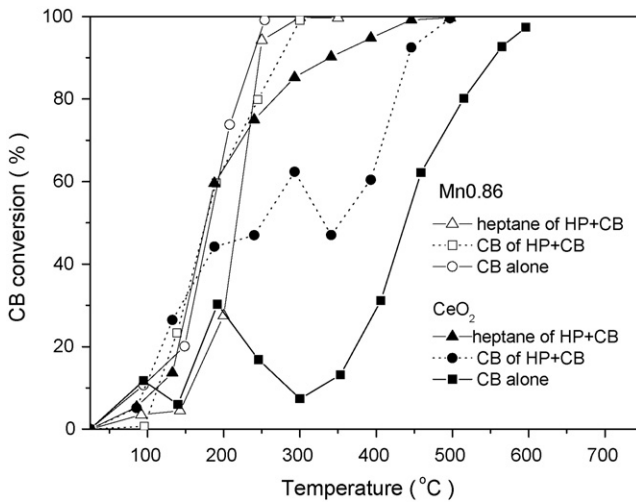
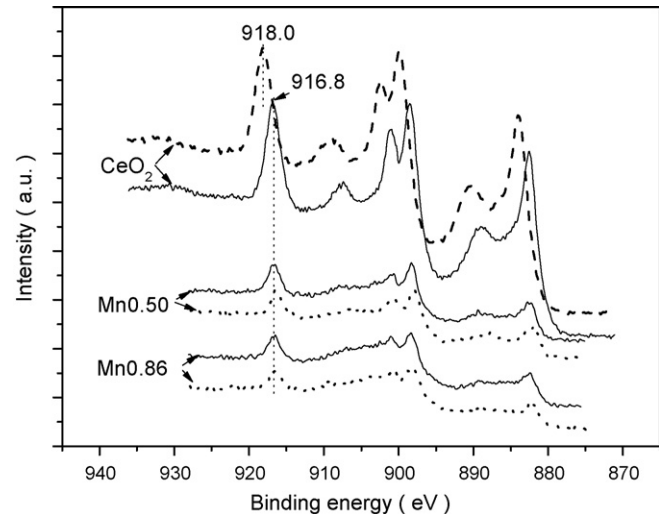


Fig. 10. The activity of CeO<sub>2</sub> (A) and MnOx(0.86)–CeO<sub>2</sub> (B) after the treatment under different conditions, gas composition: 1000 ppm CB, 10% O<sub>2</sub>, N<sub>2</sub> balance; GHSV = 15,000 h<sup>-1</sup>.



**Fig. 11.** The activity of  $\text{CeO}_2$  and  $\text{MnOx}(0.86)-\text{CeO}_2$ , CB alone: 1000 ppm CB; HP mixture: 1000 ppm CB + 1000 ppm heptane; 10%  $\text{O}_2$ ,  $\text{N}_2$  balance; GHSV = 15,000  $\text{h}^{-1}$ .

350 °C. This test was carried out after the evaluation of activity of the fresh catalysts. Stable activity can be achieved within 0.5–1 h over  $\text{MnOx}-\text{CeO}_2$  catalysts with  $\text{Mn}/\text{Ce} + \text{Mn}$  ratios of 0.86, 0.78, 0.69, 0.5, 0.27,  $\text{MnOx}$  and  $\text{CeO}_2$ , on which the stable conversions of CB within 1000 min are about 98, 84, 81, 79, 60, 45 and 19%, respectively.  $\text{MnOx}(0.86)-\text{CeO}_2$  in particular was tested for another 100 h with the conversion as high as 98%. Compared with the activity of the fresh  $\text{MnOx}-\text{CeO}_2$  catalysts shown in Fig. 4, it can be concluded that the activity drop of catalysts depends on Ce amount in catalysts; the deactivation is related to the strong adsorption of  $\text{HCl}$  or  $\text{Cl}_2$  produced from the decomposition of CB on the  $\text{CeO}_2$  surface and hence the blockade of active sites [9]. When the temperature is raised to 350 °C, the activity of catalysts does not decrease, indicating that for Cl species on active sites, the removal rate can balance dynamically the deposition rate.



**Fig. 12.** Ce 3d XPS spectra for the fresh (solid line) and used (dash line)  $\text{CeO}_2$  and  $\text{MnOx}-\text{CeO}_2$  catalysts.

Fig. 10 shows the activity of  $\text{CeO}_2$  and  $\text{MnOx}(0.86)-\text{CeO}_2$  after the treatment under different conditions.  $\text{MnOx}(0.86)-\text{CeO}_2$  is found to easily deactivate and  $T_{50\%}$  value increases from 180 to 308 °C after the first reaction run. Regeneration of the activity was investigated by feeding CB-free air or Ar over the catalyst at 350 °C. In air flow, the activity at low temperature less than 150 °C can be recovered readily to the level of the fresh catalyst, whereas one at high temperature needs longer treatment time to recover, because removal of chlorine or chloride from the surface of the used catalysts is a slow step. It can be inferred that, if the sweeping time is sufficient, the activity of the used  $\text{MnOx}(0.86)-\text{CeO}_2$  could be recovered completely. As to the treatment in Ar, however, the catalyst does not recover, possibly because the absorbed Cl cannot be removed. So, the removal of Cl species can be realized by the reaction of oxygen species with Cl species to form  $\text{Cl}_2$  (detected in

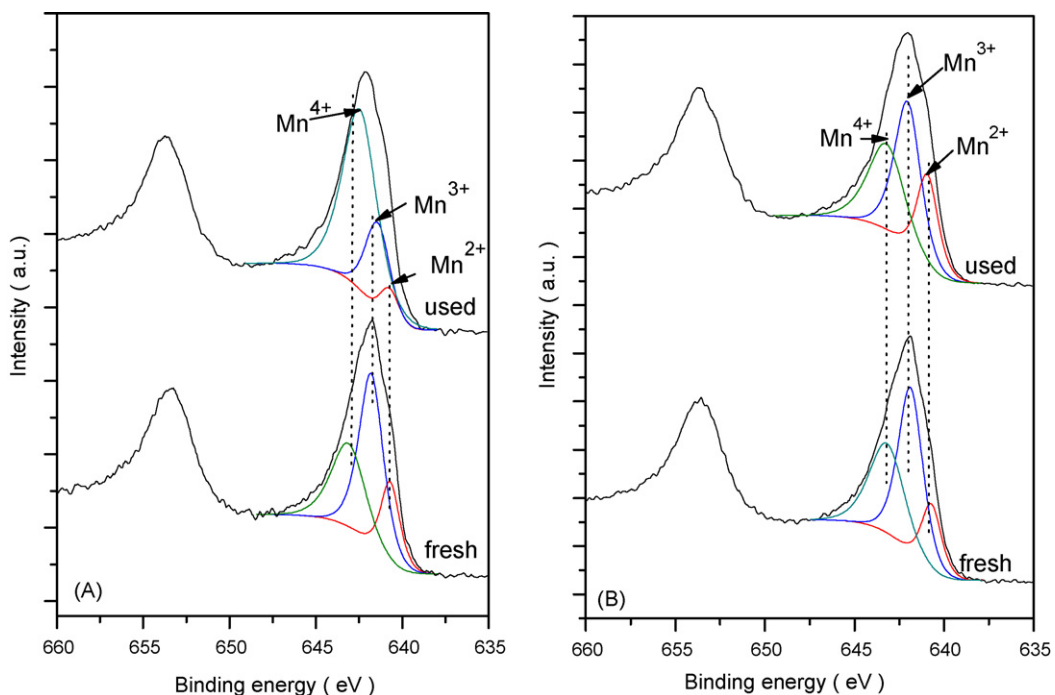


**Fig. 13.** Mn 2p XPS spectra for the fresh and used catalysts: (A)  $\text{MnOx}(0.69)-\text{CeO}_2$ ; (B)  $\text{MnOx}(0.86)-\text{CeO}_2$ .

the effluent with MC). However, the activity of the used  $\text{CeO}_2$  catalyst cannot be recovered in both air and Ar.

$\text{CeO}_2$  is active in the decomposition of CVOCs [8,9]. In the catalytic combustion of CB, CB adsorption and then C–Cl bond dissociation occur at low temperatures on  $\text{CeO}_2$  [9], and the resulting fragments can react with active oxygen to produce  $\text{CO}_2$  and  $\text{H}_2\text{O}$ . Chlorine species need be removed as  $\text{Cl}_2$  or  $\text{HCl}$  from the surface of catalysts, or chlorine species block the active sites so as to deactivate catalysts. On Pt catalysts, the adsorbed chlorine species can react with CB to form polychlorinated compounds, due

to the ability of Pt catalysts to catalyze the chlorination [40,41]. So, Pt catalysts generally presented a relative stable activity for CB combustion. Over  $\text{CeO}_2$  catalyst, no polychlorinated compounds were found in the effluent gases, and the removal of adsorbed chlorine species was promoted by elevating temperature. It may be implied that the removal of Cl species is a slow step so that it determines the catalytic combustion rate of CB. The incorporation of Mn makes more the amount of active oxygen in the structure of  $\text{MnO}_x\text{--CeO}_2$  catalysts (see Table 1) and improves the activity in CB catalytic combustion. On the other hand, the presence of Mn

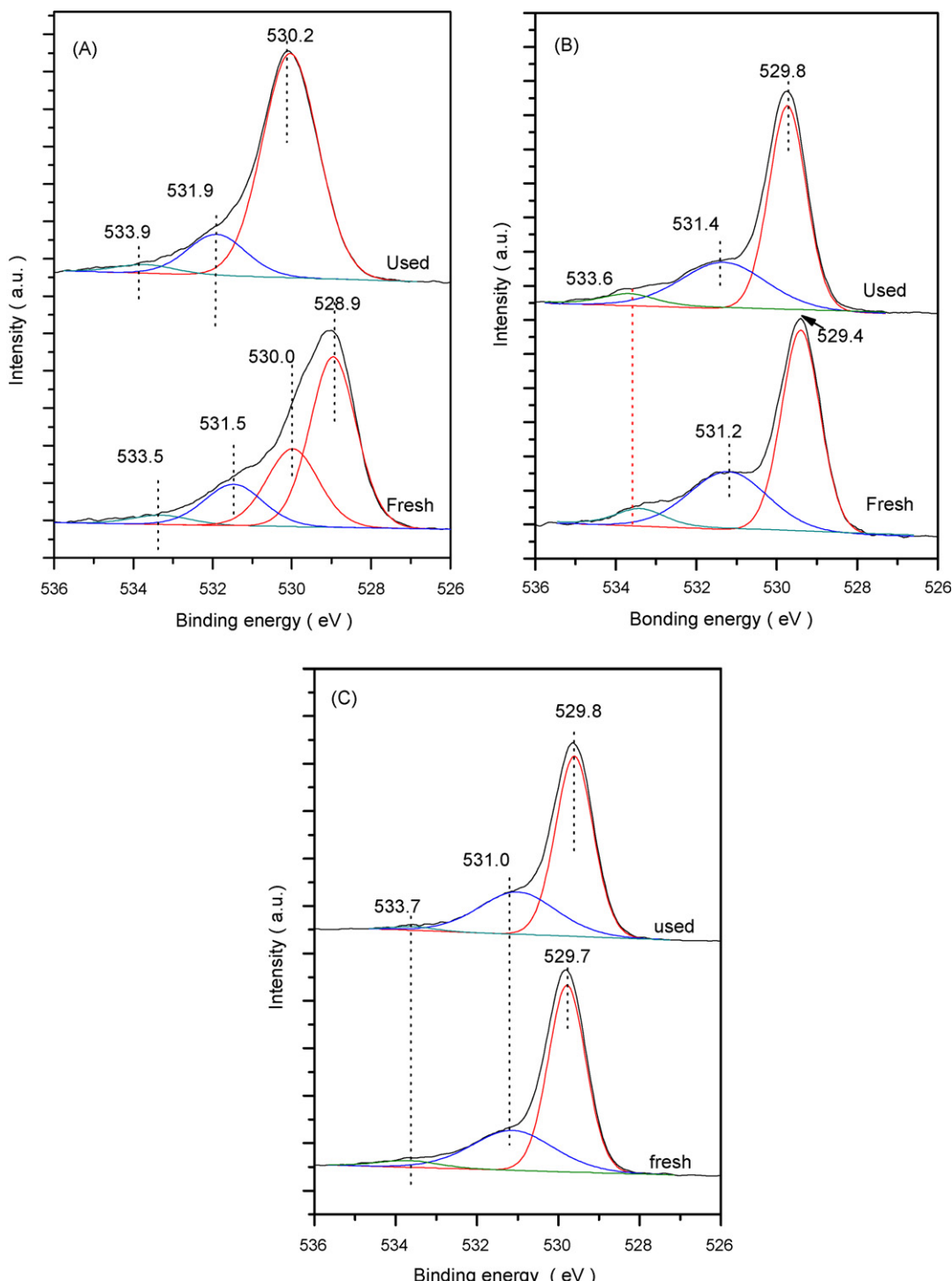


**Fig. 14.** O 1s XPS spectra of the fresh and used catalysts: (A)  $\text{CeO}_2$ ; (B)  $\text{MnO}_x(0.69)\text{--CeO}_2$ ; (C)  $\text{MnO}_x(0.86)\text{--CeO}_2$ .

significantly promotes the removal of chlorine species from the surface of  $\text{MnO}_x\text{--CeO}_2$ . For  $\text{MnO}_x(0.86)\text{--CeO}_2$ , the removal of chlorine species is rapid enough to maintain the active sites accessible to reactant molecules at 350 °C.

van den Brink reported that hydrocarbon could remove Cl species from the surface of Pt catalysts [40,41]. In this work, the effects of feeding heptane into the reaction mixture on the activity and stability were investigated. It can be seen in Fig. 11 that the conversion of CB in binary mixture on  $\text{MnO}_x(0.86)\text{--CeO}_2$  decreases at high temperature, and  $T_{99\%}$  shifts to 291 °C, indicating that the consumption of surface oxygen in the oxidation of heptane decreases oxygen species necessary to remove the adsorbed Cl species. For  $\text{CeO}_2$ , the addition of heptane decreases  $T_{99\%}$  value by 115 °C. The reaction pathway may involve a H-atom abstraction from heptane on  $\text{CeO}_2$ , which is reactive for the combination with the adsorbed Cl species to form HCl. van den Brink described this process in the catalytic combustion of CB on  $\text{Pt/Al}_2\text{O}_3$  [40]. So, the removal of the strongly adsorbed Cl species produced during the decomposition of CB can be promoted by hydrogen species from the hydrocarbon.

To obtain more insight into the promotion function by  $\text{MnO}_x$ , the physico-chemical properties of different catalysts were characterized. The results show that after being used for 1000 min at 350 °C for the combustion of CB, the specific surface area of all the  $\text{MnO}_x\text{--CeO}_2$  catalysts rarely change, no phase transformations are observed in their XRD patterns and the obvious deposit of coke on the catalyst surface was not detected by TG techniques. However, the change of XPS spectra of species on the used catalyst surface was observed. From Fig. 12, it can be seen that Ce 3d core level is formed by two series of peaks:  $3d_{5/2}$  and two very pronounced "shake-up" satellites and  $3d_{3/2}$  with the same characteristics [42]. For the deactivated  $\text{CeO}_2$ , Ce 3d level shifts substantially to higher values, whereas the spectra of Ce 3d for  $\text{MnO}_x\text{--CeO}_2$  catalysts with  $\text{Mn}/\text{Mn} + \text{Ce}$  ratio of 0.50 and 0.86 hardly change. As compared with Mn 2p core level in XPS spectra in Fig. 13 for the fresh  $\text{MnO}_x(0.50)\text{--CeO}_2$ , an increase in band intensities of  $\text{Mn}^{4+}$  (642.5 eV) of the used catalyst reveals that more Mn species are already oxidized. However, this situation does not occur for  $\text{MnO}_x(0.86)\text{--CeO}_2$ . Moreover, O 1s XPS spectra (see Fig. 14) for the fresh and used catalysts  $\text{CeO}_2$ ,  $\text{MnO}_x(0.50)\text{--CeO}_2$  and  $\text{MnO}_x(0.86)\text{--CeO}_2$ , show that O 1s level of lattice oxygen increases from 528.9 to 530.2 eV, 529.4 to 529.7 eV and 529.7 to 529.8 eV for the used  $\text{CeO}_2$ ,  $\text{MnO}_x(0.50)\text{--CeO}_2$  and  $\text{MnO}_x(0.86)\text{--CeO}_2$  catalysts, respectively. And the same trend of O 1s XPS spectra of active oxygen on these catalysts is observed. Cl 2p peak appearing at around 198 eV on XPS spectra and EDS results (not shown) confirm the presence of chlorine species on all of the used catalysts. The amount of deposited Cl is about 2.4–2.6 at.%, estimated by XPS and EDS.

Considering the continuous production of HCl and  $\text{Cl}_2$  in the process of CB combustion, the chlorination of Ce and Mn species in the used catalysts was investigated by Raman spectra. The Raman spectrum (not shown) indicates that, the bands at 177, 208  $\text{cm}^{-1}$  ( $\text{CeCl}_3$ ), 119, 327  $\text{cm}^{-1}$  ( $\text{CeOCl}$ ) [43], and 1600  $\text{cm}^{-1}$  ( $\text{MnO}_x\text{Cl}_y$ ,  $\text{MnCl}_2$ ) [44] are not observed. It is suggested that the chlorination of Ce and Mn species under the reaction condition (the excess of  $\text{O}_2$ ) proceeds so difficultly, or the oxidation of chlorinated Mn or Ce species proceeds so rapidly that the amount of chlorinated Mn or Ce is very small.

According to a significant shift of Ce 3d level of the used  $\text{CeO}_2$  catalyst, it can be deduced that the strongly electro-negative chlorine species adsorbed on  $\text{CeO}_2$  sites make the transition of charge density from Ce atom to Cl atom. The binding energy shifts of all species on surface of  $\text{MnO}_x(0.86)\text{--CeO}_2$  are slight, due to a weak adsorption of chlorine species. Therefore, the deactivation of

catalysts is related to the strong adsorption of HCl or  $\text{Cl}_2$  produced from the decomposition of CB.

From the above results, it can be concluded that oxygen species can efficiently react with the Cl species that adsorbed with moderate strength on the surface. For pure  $\text{CeO}_2$  or  $\text{MnO}_x\text{--CeO}_2$  catalysts with low amount of Mn, surface oxygen migrates readily (see the first reduction peak shown in Fig. 2), but the amount of surface oxygen is small and the adsorption of Cl species is strong. So, these catalysts need high temperature to remove the adsorbed Cl species, and present a low stable activity. There are more active oxygen species for  $\text{MnO}_x(0.86)\text{--CeO}_2$  to remove the Cl species adsorbed with moderate strength on the surface of catalysts during the reaction, so that more active sites can be accessible. Therefore, the stability of  $\text{MnO}_x\text{--CeO}_2(0.86)$  in the catalytic combustion of CB is promoted at 350 °C, due to a larger decrease in chlorine species deposit.

#### 4. Conclusion

In summary, it has been found that  $\text{MnO}_x\text{--CeO}_2$  catalysts present high activity for the low-temperature catalytic destruction of CB. The main products from CB catalytic destruction over the  $\text{MnO}_x\text{--CeO}_2$  catalysts are HCl,  $\text{Cl}_2$ ,  $\text{CO}_2$  and trace CO, and polychlorinated compounds has not been detected.  $\text{MnO}_x\text{--CeO}_2$  catalysts with high ratios of  $\text{Mn}/\text{Ce} + \text{Mn}$  present a high stable activity, which is related to their high ability to remove the adsorbed Cl species and a large amount of active surface oxygen.

#### Acknowledgements

We would like to acknowledge the financial support from National Basic Research Program of China (No. 2006AA06Z379 and No. 2004CB719500), National Natural Science Foundation of China (No. 20377012) and the Commission of Science and Technology of Shanghai Municipality (No. 05QMX1413 and No. 06 JC14020).

#### References

- [1] R. Weber, T. Sakurai, H. Hagenmeier, *Appl. Catal. B: Environ.* 20 (1999) 249.
- [2] M. Taralunga, B. Innocent, J. Mijoin, P. Magnoux, *Appl. Catal. B: Environ.* 75 (2007) 139.
- [3] S. Scirè, S. Minicò, C. Crisafulli, *Appl. Catal. B: Environ.* 45 (2003) 117.
- [4] F. Bertinchamps, M. Treinen, P. Eloy, A.M. Dos Santos, M.M. Mestdagh, E.M. Gaigneaux, *Appl. Catal. B: Environ.* 70 (2007) 360.
- [5] F. Bertinchamps, C. Gregoire, E.M. Gaigneaux, *Appl. Catal. B: Environ.* 66 (2006) 1.
- [6] M. Taralunga, J. Mijoin, P. Magnoux, *Catal. Commun.* 7 (2006) 115.
- [7] M. Guillemot, J. Mijoin, S. Mignard, P. Magnoux, *Appl. Catal. A: Gen.* 327 (2007) 211.
- [8] Q.G. Dai, X.Y. Wang, G.Z. Lu, *Catal. Commun.* 8 (2007) 1645.
- [9] Q.G. Dai, X.Y. Wang, G.Z. Lu, *Appl. Catal. B: Environ.* 81 (2008) 192.
- [10] M. Magureanu, N.B. Mandache, J. Hu, R. Richards, M. Florea, V.I. Parvulescu, *Appl. Catal. B: Environ.* 76 (2007) 275.
- [11] M. Guillemot, J. Mijoin, P. Magnoux, *Appl. Catal. B: Environ.* 75 (2007) 249.
- [12] M.E. Swanson, H.L. Greene, *Appl. Catal. B: Environ.* 52 (2004) 91.
- [13] R. Lopez-Fonseca, J.I. Gutierrez-Ortiz, A.A. Aranzabal, J.R. Gonzalez-Velasco, *Appl. Catal. B: Environ.* 41 (2003) 31.
- [14] X.T. Sayle, D. Sayle, *Phys. Chem. Chem. Phys.* 7 (2005) 2936.
- [15] M.C. Alvarez-Galvan, V.A. de la Pena, O. Shea, J.L.G. Fierro, P.L. Arias, *Catal. Commun.* 4 (2003) 223.
- [16] C.N. Costa, V.N. Stathopoulos, V.C. Belessi, A.M. Efstratiou, *J. Catal.* 197 (2001) 350.
- [17] R. Craciun, B. Nentwich, K. Hadjiivanou, H. Knözinger, *Appl. Catal. A: Gen.* 243 (2003) 67.
- [18] G. Qi, R.T. Yang, *J. Phys. Chem. B* 108 (2004) 15738.
- [19] M. Kramer, W.F. Maier, *Appl. Catal. A: Gen.* 302 (2006) 257.
- [20] J.R. Gonzalez-Velasco, A. Aranzabal, R. Lopez-Fonseca, R. Ferret, J.R. Gonzalez-Marcos, *Appl. Catal. B: Environ.* 24 (2000) 33.
- [21] R. Lopez-Fonseca, A. Aranzabal, J.I. Alvarez-Uriarte, J.R. Gonzalez-Velasco, *Appl. Catal. B: Environ.* 30 (2001) 303.
- [22] M. Machida, M. Uto, D. Kurogi, T. Kijima, *Chem. Mater.* 12 (2000) 3158.
- [23] D. Terribile, A. Trovarelli, C. De Leitenburg, A. Primavera, G. Dolcetti, *Catal. Today* 47 (1999) 133.
- [24] L. Dimesso, L. Heider, H. Hahn, *Solid State Ionics* 123 (1999) 39.

[25] F. Arena, E. Alongi, P. Famulari, A. Parmaliana, G. Trunfio, *Catal. Lett.* 107 (2006) 39.

[26] F. Arena, G. Trunfio, J. Negro, B. Fazio, L. Spadaro, *Chem. Mater.* 19 (2007) 2269.

[27] E. López-Navarrete, A. Caballero, A.R. González-Elipe, M. Ocaña, *J. Eur. Ceram. Soc.* 24 (2004) 3057.

[28] F. Kapteijn, L. Singoredjo, A. Andreini, *Appl. Catal. B: Environ.* 3 (1994) 173.

[29] F. Arena, T. Torre, C. Raimondo, A. Parmaliana, *Phys. Chem. Chem. Phys.* 3 (2001) 1911.

[30] J. Carnö, M. Ferrandon, E. Björnbom, S. Järås, *Appl. Catal. A: Gen.* 155 (1997) 265.

[31] J. Trawczynski, B. Bielak, W. Miśta, *Appl. Catal. B: Environ.* 55 (2004) 277.

[32] S.T. Hussain, A. Sayari, F. Larachi, *Appl. Catal. B: Environ.* 34 (2001) 1.

[33] H.C. Yao, Y.F. Yu Yao, *J. Catal.* 86 (1984) 254.

[34] Y. Liu, Z. Wei, Z. Feng, M. Luo, P. Yang, C. Li, *J. Catal.* 202 (2001) 200.

[35] A. Musialik-Piotrowska, B. Mendyka, *Catal. Today* 90 (2004) 139.

[36] R.W. van den Brink, P. Mulder, R. Louw, *Catal. Today* 54 (1999) 101.

[37] M. Taralunga, J. Mijoin, P. Magnoux, *Appl. Catal. B: Environ.* 60 (2005) 163.

[38] Y. Liu, M. Luo, Z. Wei, Q. Xin, P. Yang, C. Li, *Appl. Catal. B: Environ.* 29 (2001) 61.

[39] T.J. Corella, A.M. Padilla, *Appl. Catal. B: Environ.* 24 (2002) 33.

[40] R.W. van den brink, R. Louw, P. Mulder, *Appl. Catal. B: Environ.* 25 (2000) 229.

[41] R.W. van den brink, R. Louw, P. Mulder, *Appl. Catal. B: Environ.* 16 (1998) 219.

[42] A.E. Nelson, K.H. Suhulz, *Appl. Surf. Sci.* 210 (2003) 206.

[43] R.M. Lago, M.L.H. Green, S.C. Tsang, M. Odlyha, *Appl. Catal. B: Environ. Appl. Catal. B* 8 (1996) 107.

[44] D. Sarme, S. Blazewicz, M. Mermoux, P. Touzain, *Carbon* 39 (2001) 2049.